Supporting Information

Filippo Zorzi, [§,†] Emil Alstrup Jensen, [‖,¶] Murat Serhatlioglu,[¶] Silvio Bonfadini,[§] Morten Hanefeld Dziegiel,[‖,‡] Luigino Criante, [*,§] and Anders Kristensen[¶]

§ *Center for Nano Science and Technology, Istituto Italiano di Tecnologia, Via Rubattino 81, 20134, Milan, Italy*
† *Department of Physics, Politecnico di Milano, Piazza Leonardo da Vinci, 32, 20133, Milano, Italy*
‡ *Department of Clinical Medicine, Københavns Universitet, Blegdamsvej 3B 33.5, Section A DK-2200 Copenhagen, Denmark*
¶ *Department of Health Technology, Danmarks Tekniske Universitet, Ørsteds Plads, building 345C DK-2800 Kgs. Lyngby, Denmark*
‖ *Department of Clinical Immunology, Copenhagen University Hospital, Blegdamsvej 9, Section A DK-2100 Copenhagen Ø, Denmark*

*e-mail: luigino.criante@iit

S1. General rules for optofluidic system optimal design

In the literature, there are numerous microfluidic geometries capable of controlling the dynamics of a fluid, either actively (guided by various pumping systems) or passively (exploiting the principle of capillarity). Among these geometries, designs that are capable of hydrodynamic focusing (HdF) are particularly noteworthy. HdF allows precise control of fluid and particle positioning, aligning particles in a single file at the centre of the channel, regardless of their size. It is an active technique in which a fluid sheath (buffer) encloses, in a coaxial geometry, a sample fluid with a cross-sectional area that can vary from tens to a few microns, ready to enter the detection zone. Although this solution can be applied to any type of fluid, it is essential when dealing with suspension particle fluids (Newtonian and non-Newtonian such as blood), where there is a significant risk of obstruction when using traditional microfluidic solutions (small channels and/or glass capillary). Moreover, the resulting fluid-fluid interface offers enormous advantages in terms of the minimising of cell shear stress, as they are not subject to the classical parabolic velocity profile of the microfluidic flow in contact with the (semi-)rigid walls of the channel.
Therefore, in order to facilitate the use of the chip also by unskilled persons and to improve the reliability of the measurements, some general design guidelines can be applied to the manufacture of these chips. A useful first guideline is to fabricate a chip with a hydrodynamic focusing geometry that is easy to use: in our case, there are only two input channels, buffer, and sample, unlike many solutions in the literature that may require up to 6 channels in an attempt to precisely control the flow rate and sample stream. It is also desirable, especially for biological samples, that the fluidic chip can be buried in a rigid, chemically inert substrate (such as fused silica). In addition, the microchannels should have cross-sections with variable 3D geometry in the longitudinal direction that can be easily fabricated, and smooth transitions between the different parts of the chip (angles, constrictions, etc.). These features are essential to prevent dense fluids (such as blood) or cell aggregates from clogging the channels and to allow any air bubbles to easily exit from the chip. Otherwise, these problems can lead to misleading results by significantly distorting the Raman spectrum of the sample.
When using a chip that laminates more than one stream in parallel (multiplexing Raman measurements), it is also important to design it so that the distance between the two streams is not

less than a certain limit (at least 15 μm). This distance prevents the two samples from mixing by diffusion and thus ensures the consistency of the measurements.

S2. Calculations on the number of cells analyzed per minute

It is well known that the flow rate inside a channel is defined as follows:

$$Q = A \cdot v \tag{1}$$

where A is the cross-section of the channel and v is the average speed inside it. When considering the measured flow rate of 2 μl/min and a cross-section of 20×20μm (the size of the focused flow), the average speed is 8.2 cm/s. In the case of the capillary, it is possible to use the following expression in order to calculate the velocity of the fluid at a given distance from the center of the tube:

$$v(r) = v_0\left(1 - \left(\frac{2r}{d}\right)^2\right) \tag{2}$$

where d is the diameter of the tube and v_0 the speed at its center, and can be calculated from the following equation:

$$Q = \frac{1}{8}\pi d^2 v_0 \tag{3}$$

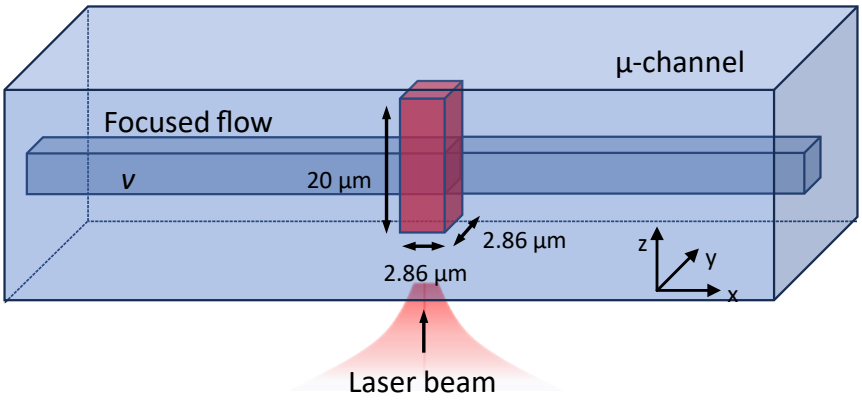

Figure SI1 Schematic drawing of the excitation voxel size

By using the same flow rate used above, it is possible to estimate the speed of the cells at around 15 μm from the wall, where the measurement is performed. When using the 100 μm capillary, the estimated speed is 0.43 cm/s. This means that using the microfluidic chip at the same flow rate the speed of cells is increased 19.3 times, compared to the capillary. Moreover, the velocity profile of the focused stream inside the chip is almost uniform. The volume of blood analyzed in a time interval t can be calculated in the following way

$$Q^* = A^* \cdot v \cdot t \tag{4}$$

where A^* is the cross-section of the voxel of the objective, which is a rectangle of size 3x20 μm^2 (when using the 50x objective the focal spot size is circular, with diameter of 2.86 μm, while the focal depth of the beam is around 20 μm) (Figure. The analyzed volume increases by the same amount as the flow speed, in particular in one minute these volumes are analyzed in the two configurations:

$$Q^*_{HF} = 0.3\ \mu l$$
$$Q^*_{cap} = 0.015\ \mu l \tag{5}$$

meaning that the throughput of the microfluidic device is also increased by the same factor as the speed. In fact, increasing the volume that flows through the voxel per unit of time means it is possible to analyze more cells for the same integration time, thus making it possible to have higher statistics while maintaining a short analysis time. Taking into account that the concentration of red blood cells in whole blood is around $5 \cdot 10^6\ 1/\mu$l,[1] the analyzed cells in one minute go from $75 \cdot 10^3$ with the capillary to $1.5 \cdot 10^6$ with the hydrodynamic focusing chip.

The interaction time between the cells and the laser beam, on the other hand, is reduced from 3 ms to 0.16 ms. Since the velocity profile of the focused stream is almost uniform, the interaction time between the cells and the laser beam is similar for all the cells.

S3. Photodegradation measurements

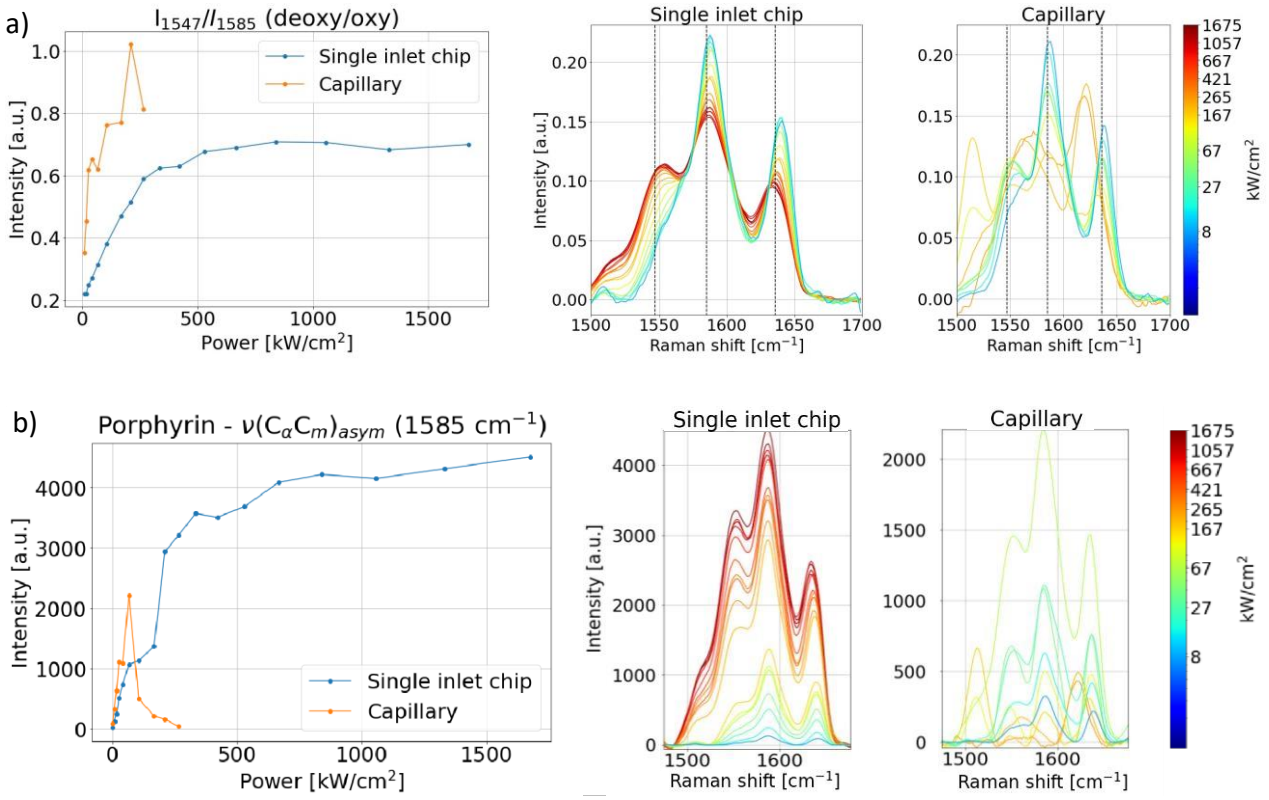

Figure SI2 Power measurements using the capillary and the LoC for two different Porphyrin peaks (δ(CmH) at 1225 cm−1, and ν(CαCm)asym at 1585 cm−1, a and b respectively). Left: amplitude of the two peaks for different excitation intensities. Right: spectra acquired with different excitation powers zoomed in the analyzed peaks regions.

Reducing the interaction time between the cells and the beam makes it possible to increase the laser power without having photodegradation of the cells. To understand the magnitude of the increase, power measurements were made with the two different device configurations, using the same blood sample. Excitation was always done with the 532 nm CW laser, however, by using neutral density filters with different absorption (THORLABS, NDK01) the laser intensity was varied from 0.8 kW/cm^2) up to 1675 kW/cm^2. The Raman signal was collected using the 50x objective, with 1 s as integration time. Then the amplitude of two different porphyrin peaks was tracked ($\delta(C_mH)$ at 1225 cm^{-1}, and $\nu(C_\alpha C_m)_{asym}$ at 1585 cm^{-1}, Figure 2 a and b respectively), and plotted as a function of laser power. In the absence of photodegradation, we expect to have a linear regime, where a doubling of the excitation intensity corresponds to a doubling of the peak amplitude, and so on. In the two configurations, the two systems show very different behaviors. With the capillary, once the threshold of about 70 kW/cm^2 is crossed, the peak amplitude collapses, almost reaching the background level. Looking at both the analyzed peaks, once the threshold is crossed their shapes completely change (Figure 2 right), due to photodegradation but also the burning of the cells, which tend to stick to the walls of the capillary. This factor hinders the measurement process, requiring the capillary to be thoroughly cleaned before it can be resumed, a very time-consuming procedure. In the case of the chip, on the other hand, we see that there is a linear regime up to a threshold of about 265 kW/cm^2, after which saturation starts to appear, a sign of laser-induced photodegradation of the cells. It can be understood how, thanks to this configuration, the laser intensity can be increased up to about 6 times without incurring into photodegradation. In addition, it can be seen that the intensity of the

peaks increases overall by 1.5 times. Thus, there is the dual advantage of increasing the statistics of the analyzed cells, due to the increased speed, and allowing faster measurements due to the increased power required for photodegradation combined with the increased Raman signal obtained from using an excitation wavelength in the visible. Moreover, unlike the capillary case, it can be seen that even above the 265 kW/cm^2 threshold the shapes of the spectra do not change (Fig. 2 a and b). Placing the blood flow away from the channel walls, even if the cells are burned these are carried away from the analysis area and do not stick to the walls. This makes the device more flexible and easier to han dle because it allows the photodegradation threshold to be accidentally exceeded without compromising the ongoing measurement. Normalizing the spectra to unit L2 norm reveals that an increased level of deoxygenation of the red blood cells occurs as the laser power is increased. The increase in the ratio between the porphyrin vibrations $\nu(C_\beta C_\beta)$ at 1547 cm^{-1} and $\nu(C_\alpha C_m)_{asym}$ at 1585 cm^{-1} is a known marker for deoxygenation of hemoglobin.

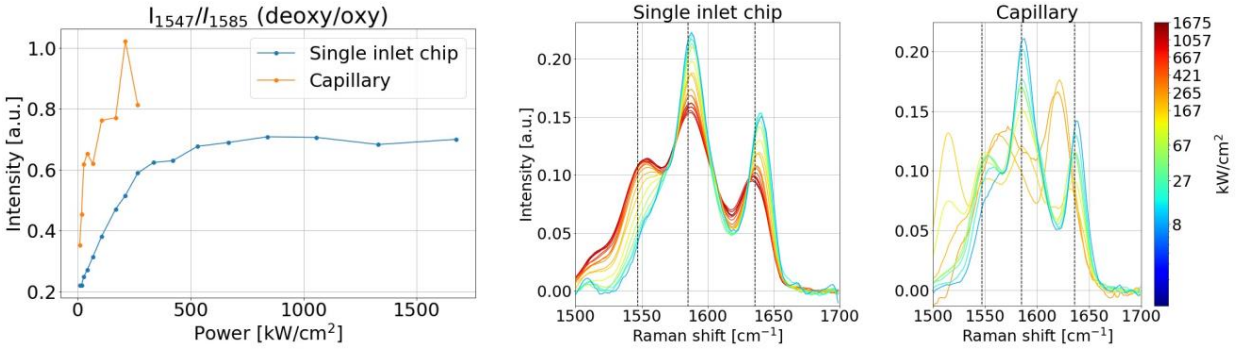

Figure SI3 The level of deoxygenation at different laser powers. The spectra are normalized to L2 unit norm.

As seen in (Fig.SI3) deoxygenation can be observed in both the capillary and chip, however, the rate is much faster in the capillary. At 27 kW/cm^2 cells in the capillary have already reached the plateau level of deoxygenation that the cells in the chip reach at 300 kW/cm^2, illustrating the vastly improved level of experimental control the chip provides.

S4. Flow rate optimization for whole blood measurements

The flow rates were adjusted so that the dimensions of the focused flow were around 15-20 µm. This provides several operational advantages: the flow dimensions were small enough to allow the larger particles of the blood's corpuscular components (leukocytes, approximately 12 µm in diameter) to pass individually while maintaining a sufficiently high flow rate to allow the cells to flow smoothly. Furthermore, this arrangement provided a good match between the excitation voxel size and the focused flow dimensions, and the centre flow was sufficiently distant away from the channel walls to avoid background signal from the fused silica (see Figure 2 in the paper). Additionally, the chip and the sample position were optimized for each measurement to maximize the signal-to-noise ratio (and minimize the integration time for each measurement).

By reducing the focused flow dimensions, the cells also moved at a higher speed, allowing for increased excitation power and the use of a visible wavelength without causing photodegradation of the sample. Once the photodegradation threshold was established, we ensured that we were

operating under conditions that maximized the available power without photodegradation, specifically at the point where the linear regime of signal increase ends.

By adjusting the sheath and sample pressure ratio it is also possible to maintain a constant diameter of the sample stream (matching the excitation voxel- approximately 20 μm), while varying the flow rate. The flow rate of whole blood could not be directly measured by flow sensors but is assumed to be proportional to the pressure of the sample inlet.

At low flow rates the rate of laser-induced deoxygenation is much faster than at high flow rates (see figure SI4a). Key parameters like flow rate and laser power should be chosen in conjunction such that the condition of the sample is under control.

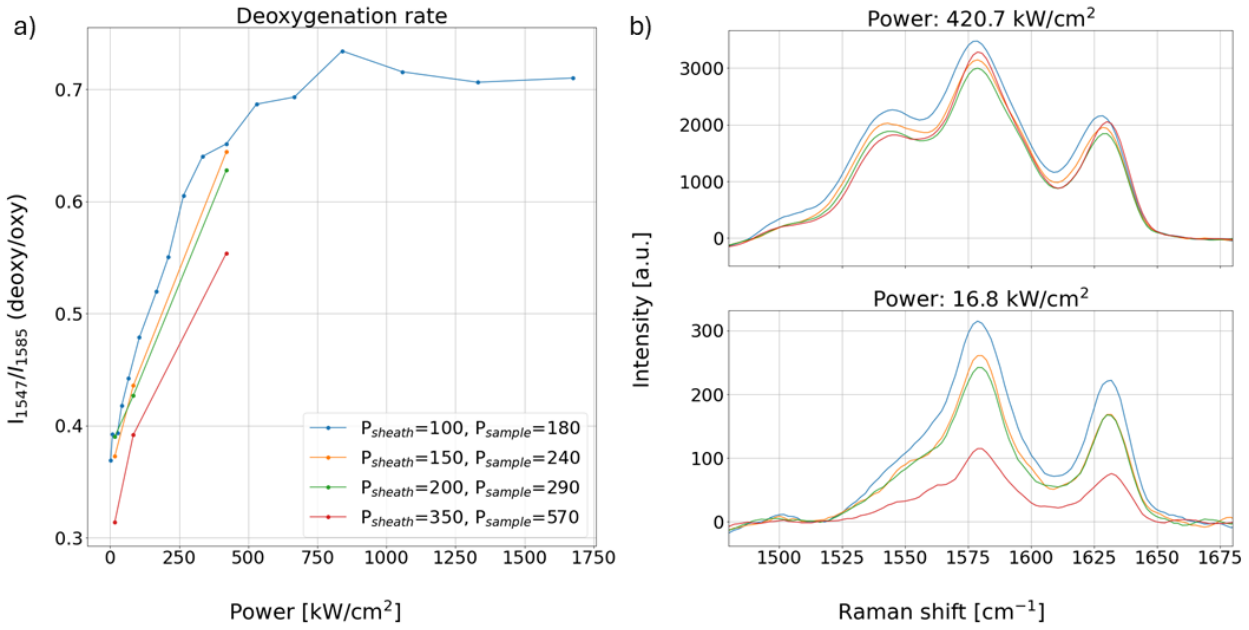

Figure SI4 a) The ratio between one of the deoxygenations and one of the oxygenation bands at different excitation laser powers and flow rates. The pressures at the sheath and sample inlets are in units of mbar. b) Corresponding Raman bands at two laser powers without normalization.

S5. Whole blood measurement

After proving the operation and effectiveness of the setup that used the two inlets chip with two test fluids, the intended operation of the device was demonstrated using blood samples. Two different types of blood were then used, specifically AB- and 0+, while PBS was used in the buffer as before (Figure SI5 a). Initially, a point-source excitation was used to excite the two samples and collect their signals. As with isopropanol and ethanol, when plotting the amplitude of various peaks, the signal from the two different samples can be clearly distinguished (Figure SI5 b).

Even when using line excitation it's possible to differentiate the contributions from the different samples from the CCD image, even with a short integration time of 1 second (Figure SI5 c). By analyzing the signal intensity along different rows of the image, it's possible to simultaneously extract the spectra of the different blood samples. Even when using a sample of interest like blood (which gives a weaker signal compared to isopropanol and ethanol), it's possible to achieve a good signal-to-noise ratio with reduced integration times (Figure SI5 d). As before, it is possible also in this case to check whether the two samples are making contact with each other by extracting a spectrum at an

intermediate row between the two of them. Moreover, also in this case, the chip can be designed to make the two streams enter in contact with each other by diffusion, and study in real time the interaction between two different samples (e.g. different blood types).

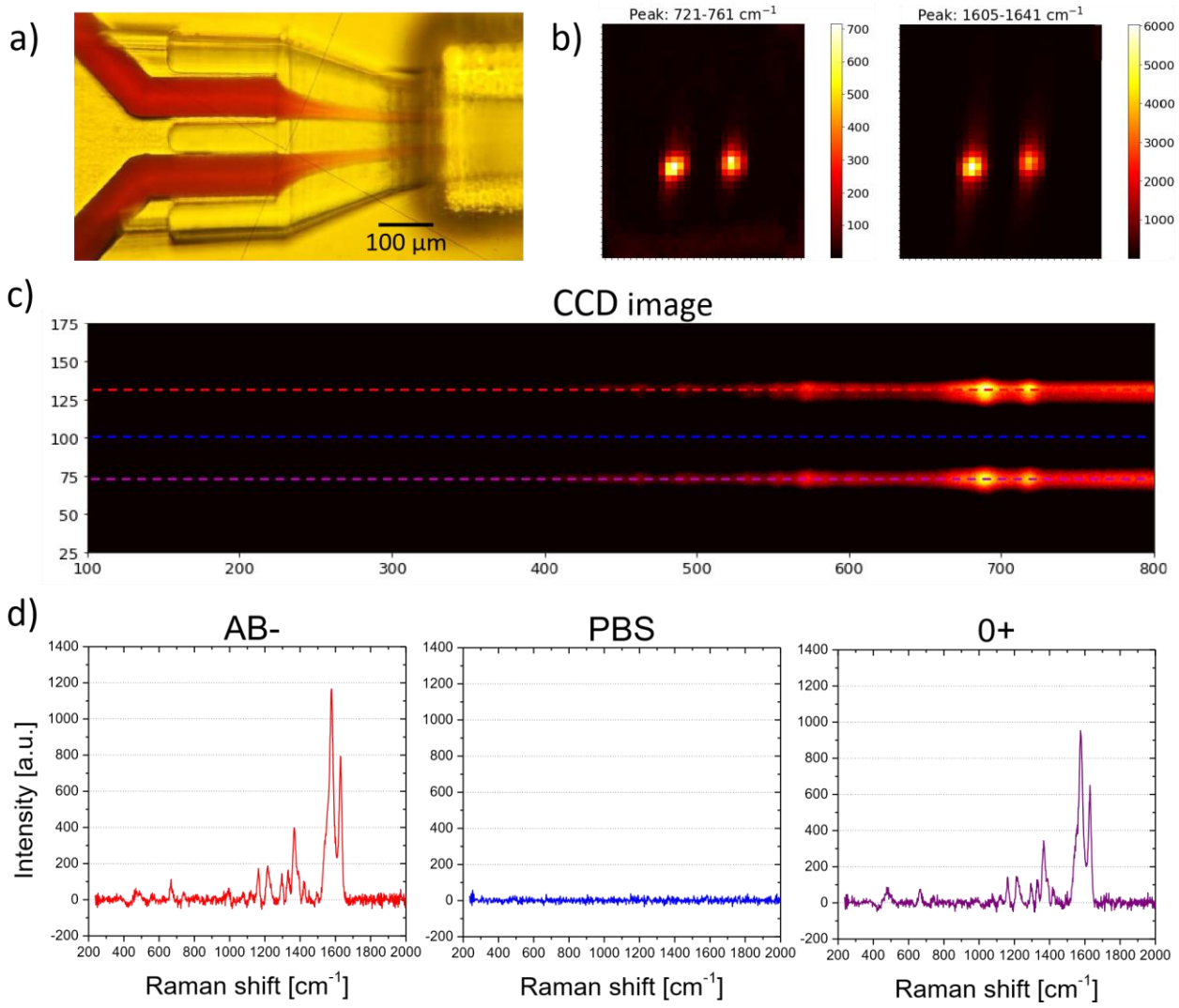

Figure SI4 a) Microscope image of the two inlets hydrodynamic focusing chip used with whole blood in the sample inlets and PBS in the buffer inlet. b) 2D maps along the cross section of the channel obtained tracking the amplitude of two peaks of whole blood. c) CCD image obtained with the double inlet chip using AB- blood (red) and 0+ blood (purple) in the two sample inlets. d) spectra obtained at different y positions of the CCD image.

References

(1) Dean, L.; National Center for Biotechnology Information (U.S.); Flying Publisher; National Library of Medicine *Blood Groups and Red Cell Antigens*; NCBI Bookshelf; NCBI, 2005; Chapter 1.